Journal of Magnetism and Magnetic Materials 580 (2023) 170898

Contents lists available at ScienceDirect

Journal of Magnetism and Magnetic Materials

journal homepage: www.elsevier.com/locate/jmmm

Research article

Decomposition of the induced magnetism degaussing problem for fast determination of currents in demagnetization coils wrapped outside an object under arbitrary external field conditions

Miroslaw Woloszyn, Jarosław Tarnawski *, Joanna Woloszyn

Gdańsk University of Technology, Gdańsk, 11/12 Gabriela Narutowicza Street, 80-233, Poland

ARTICLE INFO

Keywords:
Demagnetization problem decomposition
Electromagnetic modeling
Superposition calculus
Least squares approximations
FEM-based numerical verification magnetic analysis
Magnetic signatures

ABSTRACT

Safe passage of ships in the presence of sea mines can be ensured by limiting or reducing the ship's magnetic footprint. For vessels with plastic hulls, the main component that requires magnetic damping is the engine. Demagnetization of such an object can be achieved by wrapping it with coils and setting the direct current appropriately. For each specific geographic location, the currents in the coils can be determined iteratively from measurements of the magnetic signature in the cardinal directions. In this paper the magnetic signatures are calculated using decomposition-based approach for each coil and each component of the external field separately. Hence the overall magnetic signature of the object can be reproduced in arbitrary external magnetic field (i.e. anywhere on the Earth). Knowing the influence of each coil, it is possible to formulate the optimization task (signature minimization) and determine the currents. The presented method is verified in FEM software with the use of engine models of both symmetrical and asymmetrical shapes. Since the determination of the currents takes place as a result of solving the optimization problem, the effectiveness of obtaining the results, the speed of convergence and the dependence on initial conditions is under investigation. The effect of the model mesh size on the quality of object signature reduction is also analyzed. The developed method can be used for a real object. In that case acquiring the data then requires the measurements of the object placed inside the Helmholtz coils.

1. Introduction

A ship built of ferromagnetic materials disturbs the Earth's magnetic field in its surrounding. This disturbance is called the ship's magnetic signature. There are many papers dealing with this subject. The author of [1] explained the phenomena related to four major sources of the ship's magnetic fields. In [2], the author described passive and active reduction technics of ship's magnetic signatures generated by ferromagnetic steel, eddy currents, and corrosion currents. The mathematical models of spherical, prolate spheroidal, and semi-empirical magnetic ships and submarines were presented in [3]. The authors of [4,5] presented the mathematical model of a prolate spheroidal marine vessel with spheroidal harmonic expansion coefficients of the magnetic scalar potential. In [6–8] the authors presented a virtual magnetic model of the ship using induced and permanent magnetic dipoles. On the basis of magnetic field measurements in four cardinal directions of the ellipsoid-shaped vessel, the authors achieved a multi-dipole model which allowed to reproduce ship's magnetic signatures for an arbitrary course and measuring depth. The authors of [9] showed a good comparison of the multi-dipole model and the physical model only in North–South and South–North direction. Good compatibility of the results obtained for the real marine ship Zodiak and its multi-dipole model was presented in [10], proving that the virtual model is correct and can be used to predict ship's magnetic signatures. The decomposition of the induced and permanent magnetization of a ship was presented in [11] and [12]. The knowledge about the distributions of these two types of magnetization is useful in designing the demagnetization coil system. There are also many papers in which the authors analyzed the problem concerned with hysteresis of ship's ferromagnetic steel and the ship deperming process. These significant and complex phenomena have to be taken into account especially when reducing the vertical permanent magnetization. Numerical methods are used to analyze the deperming process. In [13–15], the authors analyzed this process using FEM with the Preisach model and demonstrated the effectiveness of this method in minimization of the ship's magnetic field. The simpler stepwise deperm method based on a single anhysteretic deperm was proposed by the authors of [16,17]. It was proved

* Corresponding author.
E-mail address: jaroslaw.tarnawski@pg.edu.pl (J. Tarnawski).

https://doi.org/10.1016/j.jmmm.2023.170898
Received 13 March 2023; Received in revised form 15 May 2023; Accepted 2 June 2023
Available online 8 June 2023

that this method is practicable and can be used instead the Flush-D deperm [18] method. In [19], the author showed that anhysteretic deperm cannot always be applied, and then an empirical method should be used. The author proposed the method based on real measurements and using the Jiles–Atherton (J–A) model. That method allowed to predict permanent magnetization of the ship after each deperm cycle. In [20], the authors presented the deperming process of the ship using coils lying on the seabed. The main advantage of that method was that the ship is not wrapped by coils, so the time of the deperming process is shorter than in classic methods. Beside deperming, another method of demagnetization is the application of coils with DC currents distributed inside the ship. In [21], the authors presented a methodology for the design of the optimal tri-axial degaussing system and the estimation of the coil currents to minimize the magnetic signature of the ship. In this methodology the magnetic signatures for each coil were calculated separately without existing external field. Next, the magnetic signature of the ship's model was calculated for the chosen Earth's magnetic field components and after adding the magnetic signatures associated with the coils with optimized currents, the minimized total signatures were finally achieved. The authors used LARS and TCS-GRR techniques for the minimization of magnetic signatures. In [22], the authors used genetic algorithm and particle swarm optimization to obtain the optimal coil's currents. The disadvantage of that method is that for each new value of the Earth's magnetic field, the ship magnetic signatures have to be measured again. Another approach was shown in [23,24], where the authors presented an efficient methodology allowing to optimize coil currents based on separate measurements of ship's magnetic fields for each coil. The authors claimed that the time of magnetic signatures measurements is shorter than the time of calculation of magnetic signatures using finite element methods. Like in [22], the disadvantage of that method is that for new values of the Earth's magnetic field, the signature for each coil has to be measured again. A special case of the demagnetization system was presented in [25], in which the authors demonstrated the possibility of selecting new values of coil currents in the case of failure of several coils. When the ship is built of plastic materials the magnetic field related to ferromagnetic devices inside it should be compensated. For this purpose the main of these devices the ship's engine is wrapped by coils in three directions to minimize the magnetic signatures. The magnetic signatures of the main engine or other devices can be calculated by using the FEM method. The coil currents intended to minimize the magnetic signature can also be calculated using FEM method. However the calculation time is relatively long in this case, as the FEM calculations have to be repeated each time for new values of the coil currents. The method of determination of currents in coils wrapped around the marine device presented in this paper is based on the methodology described in [21,22], which consists in determining the signatures associated with each, coil separately without presence of the Earth's magnetic field. The methodology of magnetic device signature calculation (without working coils) is described in detail in this paper. It is noteworthy that article leaves aside the deperming process, as it, is solely focused on the minimization of the magnetic field of a fully demagnetized ferromagnetic object, and therefore, the authors have not considered the magnetic hysteresis phenomenon. The magnetic signatures of the fully demagnetized marine device are calculated separately for only one component of the Earth's magnetic field. Then, after assembling the scaled signatures associated with each component of the magnetic field vector, the resultant signatures are obtained using superposition method for an arbitrary Earth's field. In other words, the magnetic signatures are calculated separately for each coil and each external field component. This method makes is possible to reconstruct the magnetic signatures of a marine device for an arbitrary external magnetic field. The knowledge about the device signatures related to each coil allows to determine the coil currents for minimizing the magnetic signature without necessary FEM calculations.

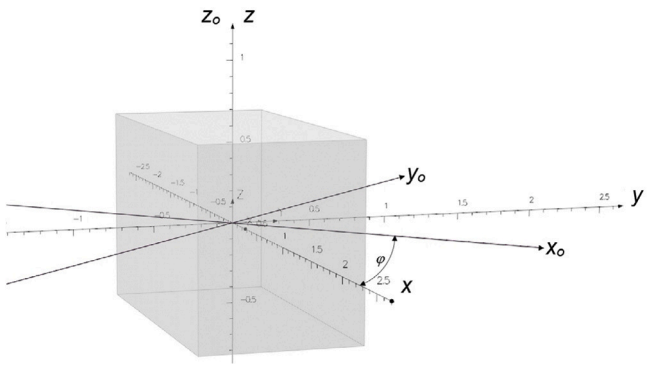

Fig. 1. Cartesian Coordinates System (CCS) and Object Coordinate System (OCS). The x-axis is oriented in the South magnetic direction.

2. Description of the magnetic field and transformations between coordinate systems

The magnetic signature of a ferromagnetic object is a complicated function of its shape, size, magnetic properties of material and an external magnetic field surrounding it. Without the presence of the external field the magnetic signature of the fully demagnetized object is null. The magnetic field of an object can be described in the rotating, Object Coordinate System (OCS — x_o, y_o, z_o) associated with an object or in the non-rotating Cartesian Coordinate System (CCS — x, y, z), Fig. 1. The induced components of the vector magnetic field of a ferromagnetic object in the OCS can be described by Eq. (1).

$$\begin{bmatrix} B_{x,o}(x_o,y_o,z_o,\varphi) \\ B_{y,o}(x_o,y_o,z_o,\varphi) \\ B_{z,o}(x_o,y_o,z_o,\varphi) \end{bmatrix} = \begin{bmatrix} k_{LL}(x_o,y_o,z_o) & k_{LT}(x_o,y_o,z_o) & k_{LV}(x_o,y_o,z_o) \\ k_{TL}(x_o,y_o,z_o) & k_{TT}(x_o,y_o,z_o) & k_{TV}(x_o,y_o,z_o) \\ k_{VL}(x_o,y_o,z_o) & k_{VT}(x_o,y_o,z_o) & k_{VV}(x_o,y_o,z_o) \end{bmatrix} \times \begin{bmatrix} B_{x,r}\cos\varphi \\ -B_{x,r}\sin\varphi \\ B_{z,r} \end{bmatrix} \tag{1}$$

where:

$B_{x,o}, B_{y,o}, B_{z,o}$ — components of the magnetic field in OCS, $B_{x,r}, B_{z,r}$-components of the reference magnetic field in CCS,

$k_{mn}(x_o, y_o, z_o)$ — magnetic distribution coefficients related to object shape, size, and magnetic properties,

$m \in (L, T, V)$, $n \in (L, T, V)$ in OCS (L — longitudinal, T — transverse, V — vertical),

φ — the angle between x and x_o axes (Fig. 1).

The magnetic distribution coefficients $k_{mn}(x_o, y_o, z_o)$ show the influence of the nth component of the object's vector magnetization into mth component of the vector magnetic field in the OCS coordinate system. The transformation from the CCS to the OCS system is given by Eq. (2). The transformation presented in Fig. 2 with application of the parameter y from Eq. (2), allows to determine the magnetic signatures on the whole x–y plane.

$$\begin{bmatrix} x_o \\ y_o \\ z_o \end{bmatrix} = \begin{bmatrix} x\cos\varphi + y\sin\varphi \\ -x\sin\varphi + y\cos\varphi \\ z \end{bmatrix} \tag{2}$$

3. The magnetic decomposition approach to fully demagnetized object

When the Earth's magnetic field is weak (of about several dozens of μT), magnetic field changes inside the ferromagnetic steel take place for any ship's course on the linear part of the magnetization characteristic [21]. Therefore, the overall magnetic signatures (B_x, B_y, B_z) of an

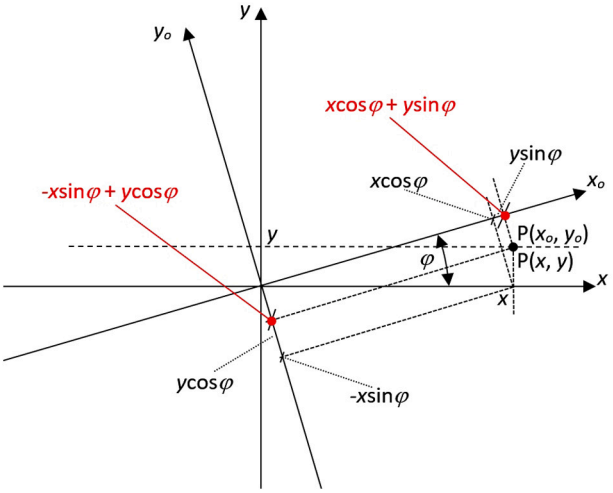

Fig. 2. Transformation of point P(x, y) in CCS into point $P(x_o, y_o)$ in OCS for arbitrary value of φ.

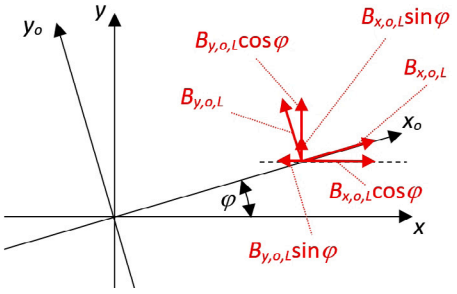

Fig. 3. Transformation of the magnetic field vector components to CCS (L-case).

object can be calculated from decomposed (partial) magnetic signatures using the superposition method. The magnetic distribution coefficients k_{mn} [26] (simplified notation for $k_{mn}(x_o, y_o, z_o)$) can be calculated using a FEM program or measured in a Helmholtz coils system. Magnetic decomposition is considered in this paper as acquiring magnetic signatures k_{mn} in three cases, in each case, only one component of the vector of the external magnetic field exists. When only the longitudinal external field exists ($\varphi = 0°$), it is possible to calculate or measure how the longitudinal magnetization of an object influences into the three components of the object's magnetic field (3). For $\varphi = 90°$ the external field works across the object and it is possible to analyze how the transverse magnetization influences into the object's magnetic field (4). Finally, when only the vertical external field exists, it is possible to calculate or measure the object's magnetic field caused by vertical magnetization (5). Once the magnetic distribution coefficients k_{mn} are known, it is possible to calculate the magnetic signatures for arbitrary direction (φ) of the object and arbitrary values of the Earth's magnetic field components B_{Ex}, B_{Ez}. The acquired (calculated using FEM or measure) magnetic signatures of an object in OCS for three above-described cases (longitudinal L, transverse T, vertical V) for different values of φ are combined using the superposition method (6) and then transformed into the CCS system (Figs. 3,4,5). The values of the external, reference magnetic field (in the OCS system) for the first decomposed L-case ($\varphi = 0°$), for the second decomposed T-case ($\varphi = 90°$), and the third decomposed V-case ($\varphi = 0°$) are respectively (50 μT, 0, 0), (0, −50 μT, 0), and (0, 0, −50 μT), as summed up in Table 1.

For better understanding of the methodology, the indices L, T and V were added respectively to these cases in the magnetic field (1) related

Table 1
Magnetic signature decomposition into datasets.

	φ	Reference fields values
Decomposed L-case	0°	(50 μT, 0, 0)
Decomposed T-case	90°	(0, −50 μT, 0)
Decomposed V-case	0°	(0, 0, −50 μT)

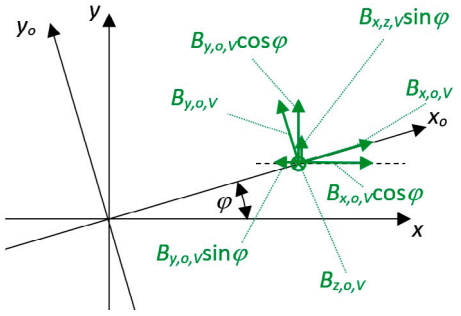

Fig. 4. Transformation of the magnetic field vector components to CCS (V-case).

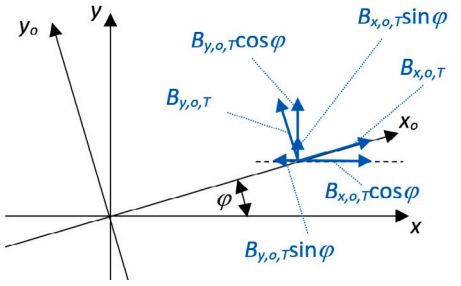

Fig. 5. Transformation of the magnetic field vector components to CCS (T-case).

to OCS.

$$\begin{bmatrix} B_{x,o,L}(x_o, y_o, z_o) \\ B_{y,o,L}(x_o, y_o, z_o) \\ B_{z,o,L}(x_o, y_o, z_o) \end{bmatrix} = \begin{bmatrix} k_{LL} & k_{LT} & k_{LV} \\ k_{TL} & k_{TT} & k_{TV} \\ k_{VL} & k_{VT} & k_{VV} \end{bmatrix} \begin{bmatrix} B_{x,r} \\ 0 \\ 0 \end{bmatrix} \tag{3}$$

$$\begin{bmatrix} B_{x,o,T}(x_o, y_o, z_o) \\ B_{y,o,T}(x_o, y_o, z_o) \\ B_{z,o,T}(x_o, y_o, z_o) \end{bmatrix} = \begin{bmatrix} k_{LL} & k_{LT} & k_{LV} \\ k_{TL} & k_{TT} & k_{TV} \\ k_{VL} & k_{VT} & k_{VV} \end{bmatrix} \begin{bmatrix} 0 \\ -B_{x,r} \\ 0 \end{bmatrix} \tag{4}$$

$$\begin{bmatrix} B_{x,o,V}(x_o, y_o, z_o) \\ B_{y,o,V}(x_o, y_o, z_o) \\ B_{z,o,V}(x_o, y_o, z_o) \end{bmatrix} = \begin{bmatrix} k_{LL} & k_{LT} & k_{LV} \\ k_{TL} & k_{TT} & k_{TV} \\ k_{VL} & k_{VT} & k_{VV} \end{bmatrix} \begin{bmatrix} 0 \\ 0 \\ B_{z,r} \end{bmatrix} \tag{5}$$

$$\begin{bmatrix} B_x(x, y, z, \varphi) \\ B_y(x, y, z, \varphi) \\ B_z(x, y, z, \varphi) \end{bmatrix} = B_{Ex}\cos\varphi \boldsymbol{A} \begin{bmatrix} k_{LL} \\ k_{TL} \\ k_{VL} \end{bmatrix} - B_{Ex}\sin\varphi \boldsymbol{A} \begin{bmatrix} k_{LT} \\ k_{TT} \\ k_{VT} \end{bmatrix} + B_{Ez} \boldsymbol{A} \begin{bmatrix} k_{LV} \\ k_{TV} \\ k_{VV} \end{bmatrix} \tag{6}$$

$$\boldsymbol{A} = \begin{bmatrix} \cos\varphi & -\sin\varphi & 0 \\ \sin\varphi & \cos\varphi & 0 \\ 0 & 0 & 1 \end{bmatrix} \tag{7}$$

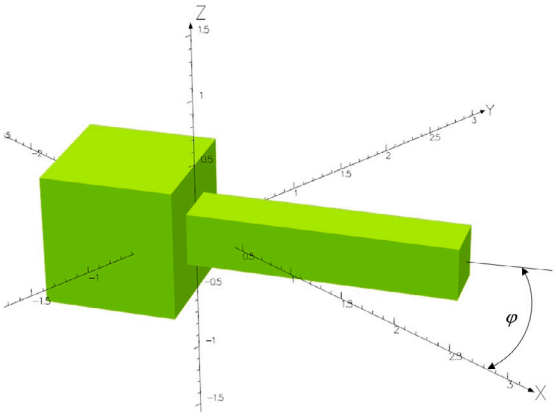

Fig. 6. The model of virtual object.

4. Numerical verification of signature determination using the decomposition-based method

To verify the presented method, simulation calculations were carried out. The virtual object selected for the simulation (Fig. 6) consisted of two cuboids with dimensions 1 m × 1 m × 1 m, and 2 m × 0.4 m × 0.4 m, connected at point (0, 0, 0). The remaining simulation parameters were: $\mu_r = 200, \varphi = 30°$, the external magnetic field $B_{Ex} = 17.101$ μT and $B_{Ez} = -46.986$ μT. The calculations were performed along a line in non-rotating CCS system (Fig. 1) for x <−10 m, 10 m>, $y = 2$ m, and z = −1.5 m. The value 50μT of the reference magnetic field $B_{x,r}$ and $B_{z,r}$ was assumed in the calculations of magnetic distribution coefficients k_{mn}. The simulations were carried out in Simulia Opera 3D [27]. The magnetic flux density distributions for three cases described in Section 3 are presented in Fig. 7. The magnetic signatures of the object model calculated in Opera from formula (6) for $\varphi = 30°$ are compared in Fig. 8.

It can be seen in this figure that the signatures are very similar to each other, with only small differences caused by numerical errors related to the approximation of magnetic field values between mesh nodes.

5. The methodology of determination of coil currents for signature silencing

When the magnetic signatures of an object are known for arbitrary angle φ and for arbitrary value of the Earth magnetic field vector, these signatures can be minimized by wrapping coils with currents around an object. The methodology for minimizing magnetic signatures is described in the upcoming steps.

5.1. Calculation or measurement of magnetic components for three cases of the external magnetic field

Based on the methodology described in the previous section, in the first step of the presented method, magnetic signatures of the object are calculated (or measured) in the presence of only one component of the external reference field.

For $\varphi = 0°$ the following magnetic distribution coefficients k_{LL}, k_{TL} and k_{VL} were calculated for one component of the magnetic field $B_{x,r}$:

$$k_{LL} = \frac{B_{x,o,L}}{B_{x,r}} \tag{8}$$

$$k_{TL} = \frac{B_{y,o,L}}{-B_{x,r}} \tag{9}$$

$$k_{VL} = \frac{B_{z,o,L}}{B_{x,r}} \tag{10}$$

and k_{LV}, k_{TV} and k_{VV} for $B_{z,r}$:

$$k_{LV} = \frac{B_{x,o,V}}{B_{z,r}} \tag{11}$$

$$k_{TV} = \frac{B_{y,o,V}}{B_{z,r}} \tag{12}$$

$$k_{VV} = \frac{B_{z,o,V}}{B_{z,r}} \tag{13}$$

For $\varphi = 90°$ the following distribution magnetic coefficients k_{LT}, k_{TT} and k_{VT} were calculated for one component of a magnetic field $-B_{x,r}$ acting across an object:

$$k_{LT} = \frac{B_{x,o,T}}{-B_{x,r}} \tag{14}$$

$$k_{TT} = \frac{B_{y,o,T}}{-B_{x,r}} \tag{15}$$

$$k_{VT} = \frac{B_{z,o,T}}{-B_{x,r}} \tag{16}$$

The presented method employs three distributions of $B_{x,o}$, $B_{y,o}$ and $B_{z,o}$ for three existing separately external fields.

5.2. Composing magnetic signatures of the Earth's magnetic field (for arbitrary geographical location)

In the next step, according to Eq. (6), three components of object's signatures are then calculated for a new value of the Earth's magnetic field $(B_{Ex}, 0, B_{Ez})$ based on calculated coefficients $k_{LL} \div k_{VV}$, which are dimensionless. Note that the denominators in formulas (8) ÷ (16) include the values of the reference magnetic field $B_{x,r}$ and $B_{z,r}$. To obtain the magnetic signatures of the object in a chosen geographical location, the coefficients should be multiplied by the Earth's magnetic field components at this location.

5.3. Acquisition of magnetic signatures of an object related separately to each coil without presence of an external field

In the third step the magnetic signatures of the object are calculated separately for each coil without the presence of the external field. Here, an assumption has been made that three coils are wrapped around the object. It can be determined how the coil's current in each coil affects the magnetic signature of an object in L, T and V directions. The distributions of nine magnetic coefficients are calculated for three reference currents (ampere-turns): longitudinal I_L, transverse I_T and vertical I_V.

$$k_{Lx} = \frac{B_{cx,o,L}}{I_L} \tag{17}$$

$$k_{Ly} = \frac{B_{cy,o,L}}{I_L} \tag{18}$$

$$k_{Lz} = \frac{B_{cz,o,L}}{I_L} \tag{19}$$

$$k_{Tx} = \frac{B_{cx,o,T}}{I_T} \tag{20}$$

$$k_{Ty} = \frac{B_{cy,o,T}}{I_T} \tag{21}$$

$$k_{Tz} = \frac{B_{cz,o,T}}{I_T} \tag{22}$$

$$k_{Vx} = \frac{B_{cx,o,V}}{I_V} \tag{23}$$

$$k_{Vy} = \frac{B_{cy,o,V}}{I_V} \tag{24}$$

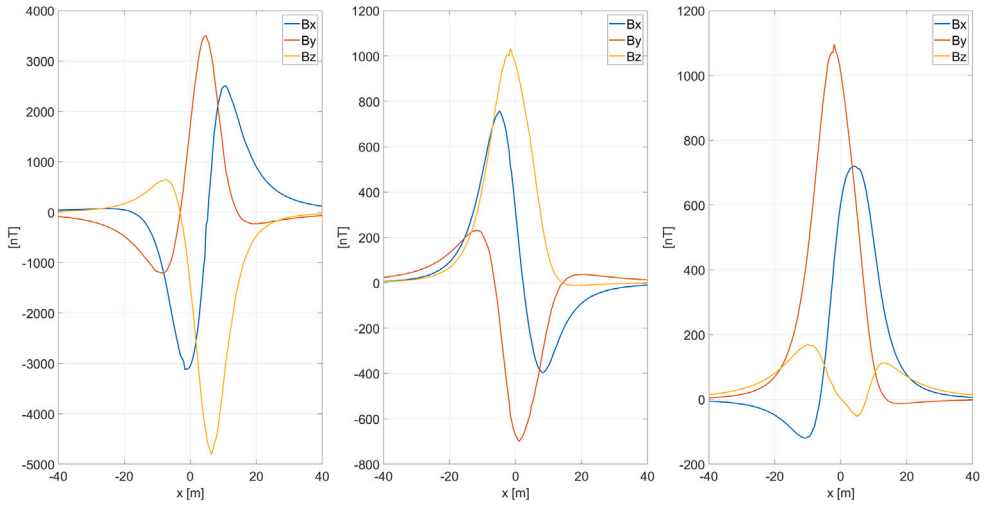

Fig. 7. Magnetic flux density for the object model: left L-case, middle T-case, right V-case.

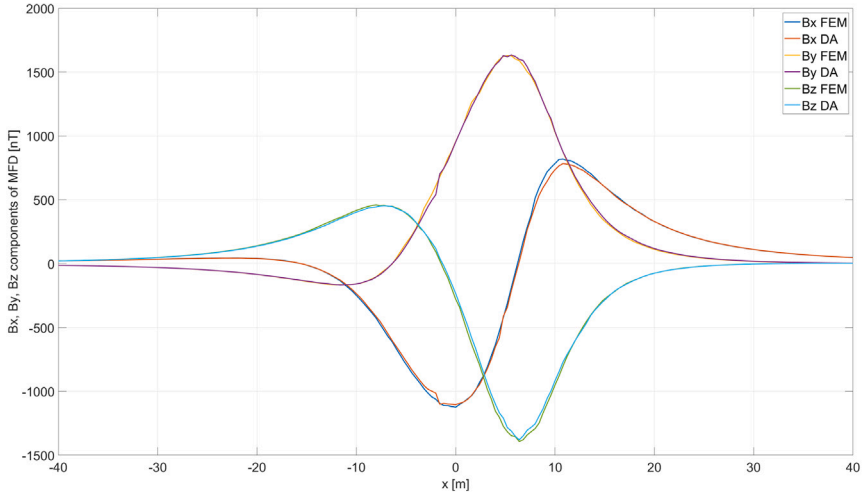

Fig. 8. Comparison between the reference signatures (FEM) and signatures calculated with the decomposed approach (DA).

$$k_{Vz} = \frac{B_{cz,o,V}}{I_V} \tag{25}$$

where: $B_{cx,o,n}, B_{cy,o,n}, B_{cz,o,n}$ — are the magnetic field components in OCS generated by the currents of each coil, n - (L, T, V).

When the coil currents are constant the magnetic signatures in OCS are independent of φ. However, they should be finally transformed to the CCS system.

5.4. Calculation of ampere-turn current values for coils wrapping the object for signature minimization

In the fourth step, the values of ampere-turn currents of three coils for minimization of object signatures are calculated or measured. The optimized $(B_{Opx}, B_{Opy}, B_{Opz})$ components of object signatures related to the induced magnetization and optimal coil's currents $I_{L1,\varphi}, I_{T1,\varphi}$ and $I_{V1,\varphi}$ for arbitrary value of φ are given by (26):

$$\begin{bmatrix} B_{Opx}(x,y,z,\varphi) \\ B_{Opy}(x,y,z,\varphi) \\ B_{Opz}(x,y,z,\varphi) \end{bmatrix} = \begin{bmatrix} B_x(x,y,z,\varphi) \\ B_y(x,y,z,\varphi) \\ B_z(x,y,z,\varphi) \end{bmatrix} + \boldsymbol{A} \begin{bmatrix} k_{Lx} & k_{Tx} & k_{Tx} \\ k_{Ly} & k_{Ty} & k_{Vy} \\ k_{Lz} & k_{Tz} & k_{Vz} \end{bmatrix} \begin{bmatrix} I_{L1,\varphi} \\ I_{T1,\varphi} \\ I_{V1,\varphi} \end{bmatrix} \tag{26}$$

5.5. Optimization criterion formulation

The values of ampere-turn currents allowing signature damping are calculated based on the following minimization criterion (27)

$$min \sum_{n=1}^{N} \sqrt{B_{Opx,n}^2 + B_{Opy,n}^2 + B_{Opz,n}^2} \tag{27}$$

where: N — number of points representing the magnetic field.

The optimization problem (fifth step) defined by (27) can be solved with a nonlinear least-squares (nonlinear data-fitting) algorithm. In general, the least squares approach consist in determining the vector containing decision variables that is a minimizer to the criterion being a sum of squares, optionally taking into account possibly some constraints. In the analyzed case the decision variables are the currents in coils with respect to constraints and the minimized sum of squares for total magnetic field.

6. Verification

Two different types of marine engines were used in verification process (Fig. 9). The results of minimization of magnetic signatures of the objects based on the data gathered along line $(x, 0, z_o)$ are shown

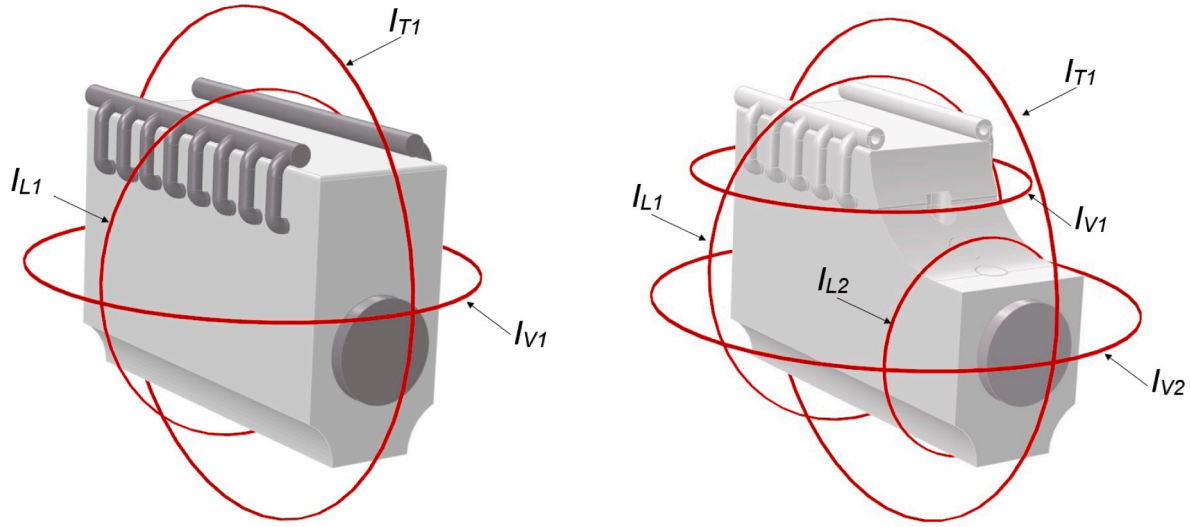

(a) symmetrical marine engine A. **(b)** asymmetrical marine engine B.

Fig. 9. Numerical models of engines for verification purposes.

in this paper for $\varphi = 0°$ and $\varphi = 90°$. Based on (26) the total magnetic field components for $\varphi = 0°$ are:

$$\begin{bmatrix} B_{Opx}(x,y,z,0°) \\ B_{Opy}(x,y,z,0°) \\ B_{Opz}(x,y,z,0°) \end{bmatrix} = \begin{bmatrix} B_{Ex}k_{LL} + B_{Ez}k_{LV} \\ B_{Ex}k_{TL} + B_{Ez}k_{TV} \\ B_{Ex}k_{VL} + B_{Ez}k_{VV} \end{bmatrix} + \begin{bmatrix} k_{Lx} & k_{Tx} & k_{Vx} \\ k_{Ly} & k_{Ty} & k_{Vy} \\ k_{Lz} & k_{Tz} & k_{Vz} \end{bmatrix} \begin{bmatrix} I_{L1,0°} \\ I_{T1,0°} \\ I_{V1,0°} \end{bmatrix} \tag{28}$$

while for $\varphi = 90°$ they are:

$$\begin{bmatrix} B_{Opx}(x,y,z,90°) \\ B_{Opy}(x,y,z,90°) \\ B_{Opz}(x,y,z,90°) \end{bmatrix} = \begin{bmatrix} -B_{Ex}k_{TT} - B_{Ez}k_{TV} \\ -B_{Ex}k_{LT} + B_{Ez}k_{LV} \\ -B_{Ex}k_{VT} + B_{Ez}k_{VV} \end{bmatrix} + \begin{bmatrix} -k_{Ly} & -k_{Ty} & -k_{Vy} \\ k_{Lx} & k_{Tx} & k_{Vx} \\ k_{Lz} & k_{Tz} & k_{Vz} \end{bmatrix} \begin{bmatrix} I_{L1,90°} \\ I_{T1,90°} \\ I_{V1,90°} \end{bmatrix} \tag{29}$$

As can be seen in Fig. 9 the engines are symmetrical regarding x–z plane, so $B_{ty} = 0$ for $\varphi = 0°$ and $\varphi = 90°$. The numerical models of the engines were built in Opera 3D [27]. The size parameters of the ship engine A model are: length 2.9 m, width 1 m and height 1.9 m. The relative magnetic permeability equal to $\mu_r = 200$ and the isotropy of engine material were assumed in the numerical analysis. Three coils were wrapped around the engine A for compensation of horizontal, vertical, and transverse magnetic field of the engine. The size of the ship engine B is similar to that of engine A but its upper part is cut out in front. Due to its asymmetrical shape in y–z plane, five coils were used for engine B. For numerical verification both engine models were placed in the external magnetic field $B_{Ex} = 17.101$ μT and $B_{Ez} = -46.986$ μT.

The basic research was carried out using the default mesh parameters (calculation time: 10 min and 50 s). Moreover, a decision was made to carry out calculations based on higher-resolution data (calculation time: 1 day, 8 h, 13 min and 20 s) to check whether the optimization result is influenced by the accuracy of the FEM calculation. The details of Opera FEM simulation parameters used for the verification are gathered in Table 2.

The complete list of numerical experiments used to verify the presented method can be found in the Table 3.

Table 2
FEM parameters.

Number of	Standard mesh parameters	High mesh parameters
active elements	9,555,657	99,159,671
nodes	1,759,497	17,216,682
equations	1,580,115	16,364,441
non-zeros	12,748,571	132,138,692

Table 3
List of numerical verification experiments.

Numerical experiment	Type of engine	Angle φ [°]	Mesh size
E1	A	0	Standard
E2	A	90	Standard
E3	B	0	Standard
E4	B	90	Standard
E5	B	0	High
E6	B	90	High

6.1. Verification of the method — numerical experiments E1, E2

The magnetic signatures of the engine in scenario E1 for $\varphi = 0°$ were calculated according to the above described five steps procedure. The magnetic signatures for each component of the external field for z = −10 m are presented in Figures A.1a, A.2a, A.3a, and A.4a diagrams, while the engine model for each external field and for I_L and for I_V are shown in Figures A.1b, A.2b, A.3b, and A.4b. The magnetic isoclines in Figures A.1c, A.2c, A.3c, A.4c, A.1d, A.2d, A.3d, and A.4d illustrate the distribution of obtained magnetic field around engine for each examined case.

The verification of this method for $\varphi = 0°$ is shown in Fig. 10. The ampere-turns for this case (Table 4) are $I_{L1,\varphi=0°} = 22,4$ At and $I_{V1,\varphi=0°} = 36,1$ At. The minimized signatures values are less than 1 nT. The calculation time for determining optimal ampere-turn currents was less than one second for both scenarios.

The magnetic signatures of the engine for $\varphi = 90°$ were also calculated for all five steps. The final result is presented in Fig. 11. The ampere-turns for this case (Table 5) are $I_{T1,\varphi=90°} = 11.2$ At and $I_{V1,\varphi=90°} = 36.1$ At. It can be seen that for $\varphi = 0°$ and $\varphi = 90°$ the values of the currents of the vertical coil are practically the same. The magnetic signatures of the engine are also dumped in this case. The biggest value of the reduced field is less than 1 nT.

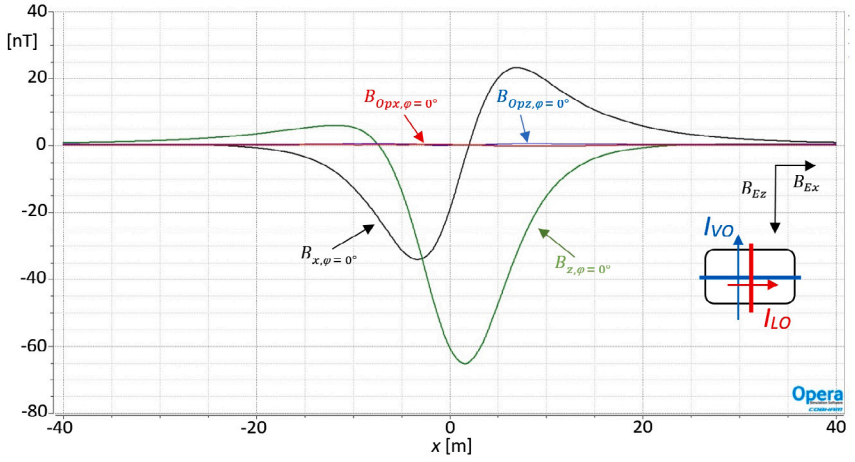

Fig. 10. Verification scenario E1 for $\varphi = 0°$.

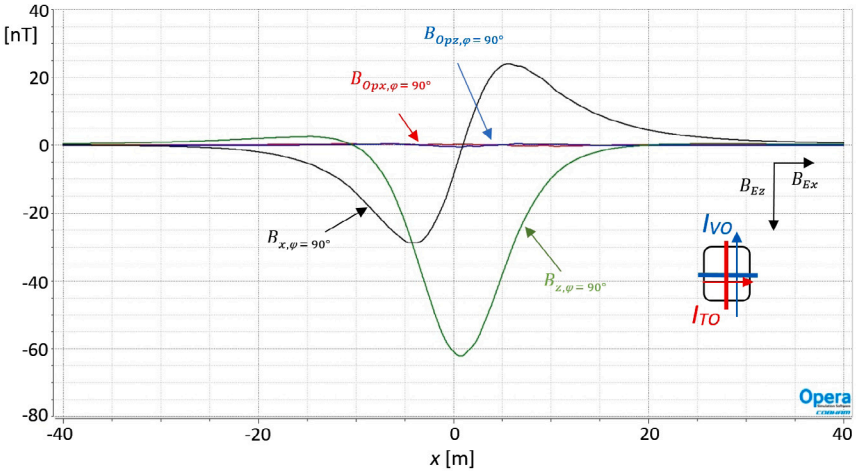

Fig. 11. Verification scenario E2 for $\varphi = 90°$.

Table 4
The results of scenario E1 — ampere-turns of coil currents for $\varphi = 0°$.

Coil current	Value [At]
$I_{L1,\varphi=0°}$	22.396
$I_{T1,\varphi=0°}$	0
$I_{V1,\varphi=0°}$	36.076

Table 5
The results of scenario E2 — ampere-turns of coil currents for $\varphi = 90°$.

Coil Current	Value [At]
$I_{L1,\varphi=90°}$	0
$I_{T1,\varphi=90°}$	11.168
$I_{V1,\varphi=90°}$	36.045

6.2. Verification of the method — numerical experiments E3, E5

For the asymmetrical engine B and angle $\varphi = 0°$ (numerical case E3 and E5), the magnetic signatures and calculations of ampere-turn currents were carried out using the same methodology but different mesh size. The final results are shown in Figs. 12 and 13 while determined coil currents are listed in Table 6. The minimization of the magnetic signatures for scenario E3 resulted in the maximum error of 0.45 nT (Fig. 14) but scenario E5 with higher-resolution mesh reduced this error to 0.2 nT (Fig. 13). This better result however, was obtained at the cost of significantly longer computation time.

Table 6
The results of scenarios E3 and E5 — ampere-turns of coil currents for $\varphi = 0°$.

Coil Current	E3 results [At]	E5 results [At]
$I_{L1,\varphi=0°}$	16.863	17.654
$I_{L2,\varphi=0°}$	9.038	7.18
$I_{T1,\varphi=0°}$	0.058	0.019
$I_{V1,\varphi=0°}$	14.345	19.230
$I_{V2,\varphi=0°}$	22.876	18.9999

6.3. Verification of the method — numerical experiments E4, E6

For the asymmetrical engine and angle $\varphi = 90°$ (numerical cases E4 and E6) the magnetic signatures and calculations of ampere-turn currents were carried out using the same methodology but different mesh size. The final results are shown in Figs. 15 and 16 while determined coil currents are listed in Table 7. The minimization of the magnetic signatures for scenario E4 resulted in the maximum error to 1.7 nT (Fig. 17) but scenario E6 with higher-resolution mesh size reduced this error to 0.9 nT (Fig. 16). Like in the previous case better results were obtained at the cost of significantly longer computation time.

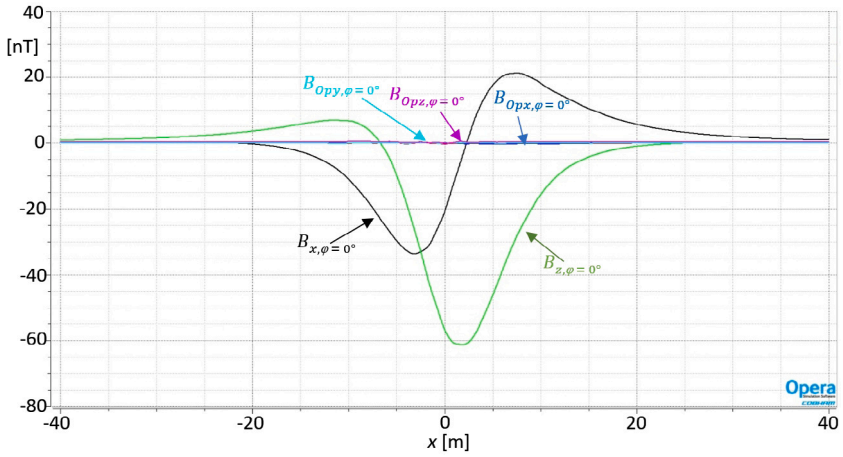

Fig. 12. Verification scenario E3 for $\varphi = 0°$.

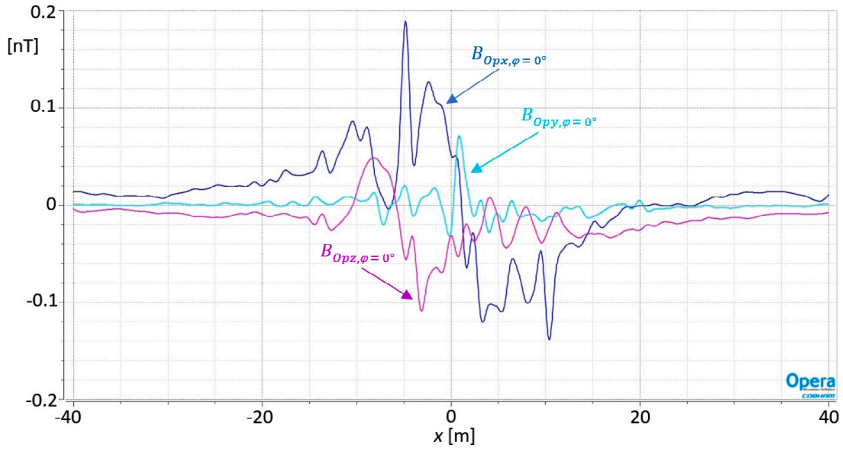

Fig. 13. Verification scenario E5 for $\varphi = 0°$.

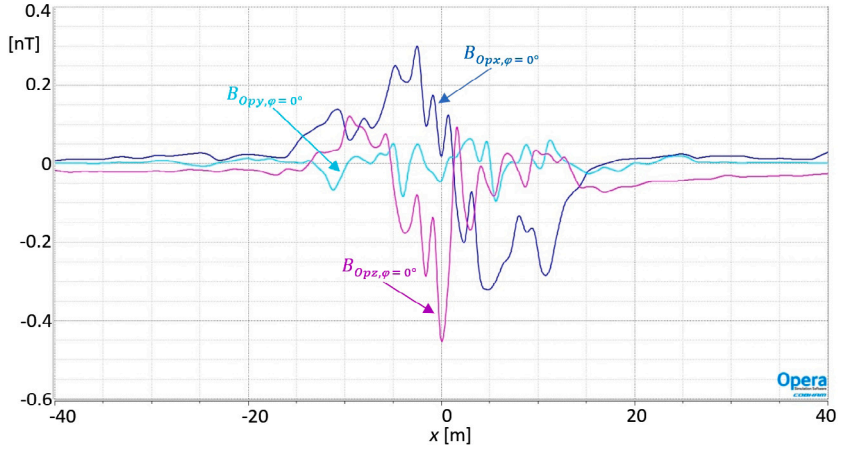

Fig. 14. Verification scenario E3 for $\varphi = 0°$ (differences).

6.4. Comments on signature minimization results

For the type A engine, the results of minimizing the magnetic signatures below 1 nT were obtained even using a standard mesh. However, for the type B engine, the errors were at a higher level and to study them calculations were performed using two different mesh sizes: standard and higher-resolution. In this case, the use higher-resolution mesh enabled to obtain the maximum error below 1 nT, i.e., similar to that observed for case A. This can be considered a satisfactory result which clearly confirms the correctness of the presented method. The optimal values of coils ampere-turns were calculated basis on distribution of magnetic field along one line x (y = 0). The distribution of the magnetic field B_x, B_y and B_z on surface x–y without coil currents are presented in Fig. B.1, B.3, B.5. The distribution of the magnetic field with coil currents are presented in Fig. B.2, B.4, B.6. The maximum value of the magnetic flux density for the silenced engine A is less than

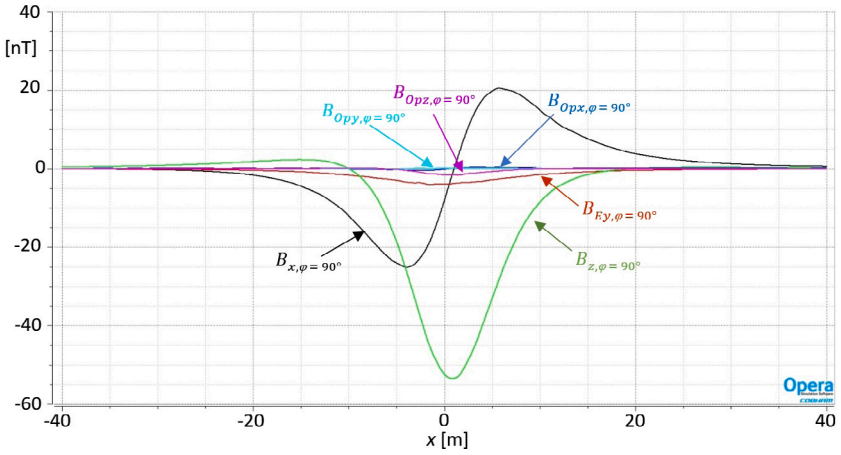

Fig. 15. Verification scenario for E4 $\varphi = 90°$.

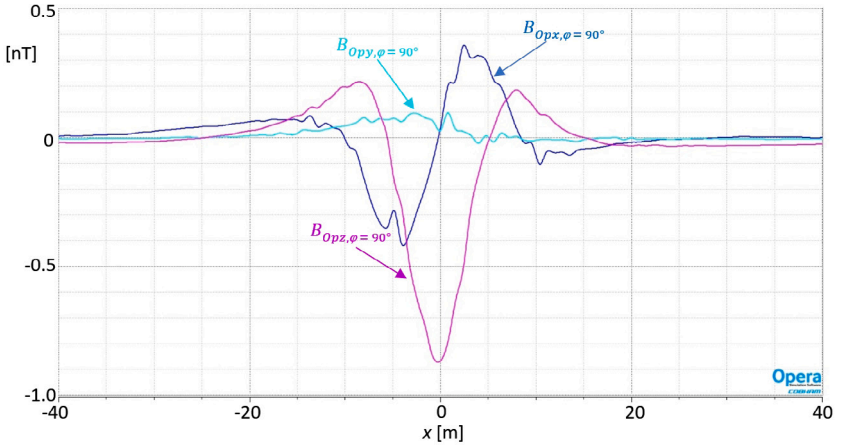

Fig. 16. Verification scenario E6 for $\varphi = 90°$.

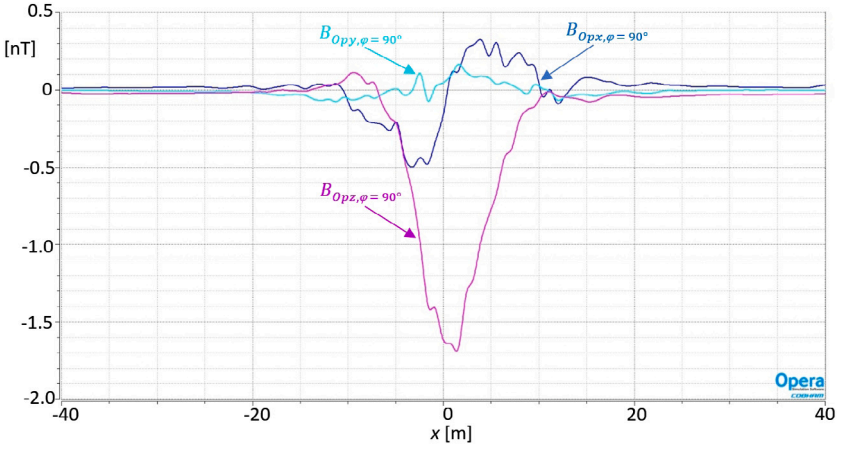

Fig. 17. Verification scenario E4 for $\varphi = 90°$ (differences).

1 nT for B_{Opx} (Fig. B.2) and B_{Opy} (Fig.B.4), and less than 2 nT for B_{Opz} (Fig. B.6).

6.5. The analysis of optimization convergence and dependence on initial values

The lsqnonlin function [28], available in the Matlab 2021 package, can be used to determine the optimal ampere-turn values. The lsqnonlin uses the Trust-Region-Reflective Least Squares Algorithm. Naturally, this algorithm is also available in other packages, libraries and languages such as, Python [29], Ceres [30] and many others. Correct solutions were obtained even using the Nonlinear GRG Solver available in MS Excel [31]. Non-gradient methods such as genetic algorithms or evolutionary strategies for instance can be applied to solve the presented optimization problem but in that case the computation time is expected to be significantly longer. Gradient methods, such as lsqnonlin

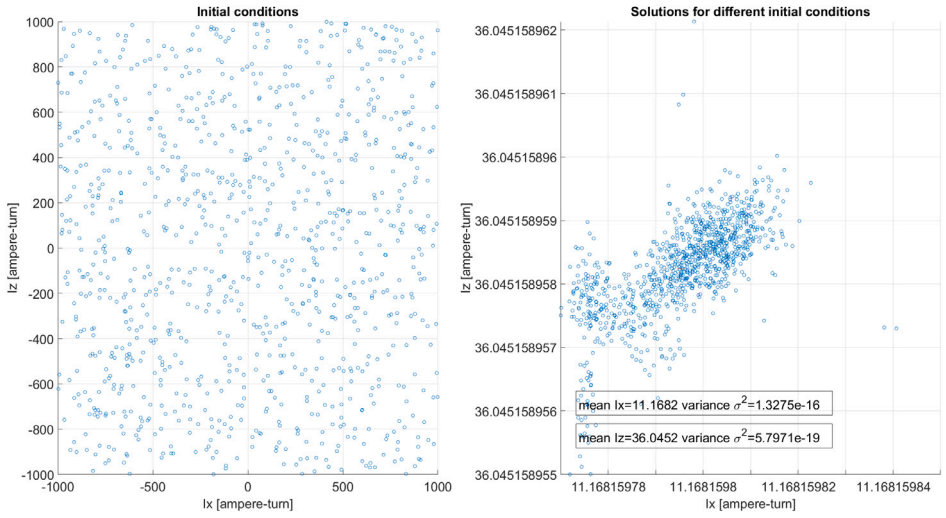

Fig. 18. Optimization dependence on initial values.

Table 7
The results of scenarios E4 and E6 — ampere-turns of coil currents for $\varphi = 90°$.

Coil Current	E4 results [At]	E6 results [At]
$I_{L1,\varphi=90°}$	−4.013	−4.197
$I_{L2,\varphi=90°}$	7.125	7.536
$I_{T1,\varphi=90°}$	10.421	10.460
$I_{V1,\varphi=90°}$	20.962	20.378
$I_{V2,\varphi=90°}$	16.562	16.948

are fast, but they are prone to getting stuck in local minima. The assessment of the usefulness of this method should be preceded by an analysis of the impact of initial conditions. Therefore, the procedure randomizing 1000 times the initial conditions from the permissible current range for simulation scenario E2 was carried out, as shown in Fig. 18. The obtained results were all very close to each other for extremely different starting conditions. The convergence of the optimization process is reported in Fig. 19. The presented results mean that the optimization problem is well conditioned. They also mean that the algorithm does not run the risk of getting stuck in local minima, hence the use of the gradient method will bring a good result with low computational effort and high computation speed. One thousand calls of the Matlab 2021 version optimization procedure running on desktop PC (CPU i7-8700, 16 GB RAM) with different initial conditions took 156 s. Compared to FEM methods, the speed of calculations as well as the universality and availability of computational tools is the advantage of the presented approach.

7. Conclusions

Magnetic signature compensation for one specific geographic location can be achieved in a practical way by iteratively adjusting the coil currents based on measurement in cardinal directions. This article presents a magnetic decomposition-based approach to determining the magnetic signatures of a ferromagnetic object. The decomposition involves obtaining signatures, by measurement or calculation, separately for each component of the external field directed along, across and vertically toward the object. Those separate signatures for external field component, can then be used to determine the signature of the entire object for its arbitrary course and arbitrary values of the Earth's magnetic field.

In order to verify the magnetic decomposition method, signatures were determined for individual components of the Earth's magnetic field, and transformed from the object-related system to the Cartesian system. Then, they were assembled and compared with the reference signatures obtained directly from the FEM Opera software.

Based on the magnetic signatures of the object for a given Earth's field and the signature associated with each individual coil wrapped around the object, the values of the currents in the coils ensuring the minimization of the Earth's magnetic field disturbance were determined by optimization.

The signature minimization process was verified using two simulated marine engines in the form of coil-wrapped ship engines and two different ship courses. The input data came from the FEM Opera software, and the method presented in the article was implemented outside the FEM, which made it possible to determine very quickly the values of currents in the coils that minimize the magnetic signatures of the engine. In the classical approach, FEM calculations are performed for every arbitrary Earth's magnetic field. Hence the optimization procedure results in a lengthy computational process. The convergence of the optimization method and its dependence on initial conditions were also investigated, as well as the effect of mesh density on the quality of the obtained results.

For objects with a more complex and asymmetrical shape, a larger number of coils wrapped around an object and a larger number of data related to magnetic signatures may be required to minimize the magnetic signature. The issue of determining the appropriate number of coils and their arrangement is a separate research and engineering problem, but the presented method is universal because it allows to consider arbitrary number of coils and signature data.

CRediT authorship contribution statement

Miroslaw Woloszyn: Conceptualization, Methodology, Formal analysis, Investigation, Resources, Writing – original draft, Writing – review & editing. **Jarosław Tarnawski:** Methodology, Software, Formal analysis, Investigation, Data curation, Writing – original draft, Writing – review & editing. **Joanna Woloszyn:** Supervision, Writing – review & editing.

Declaration of competing interest

The authors declare that they have no known competing financial interests or personal relationships that could have appeared to influence the work reported in this paper.

Data availability

Data will be made available on request.

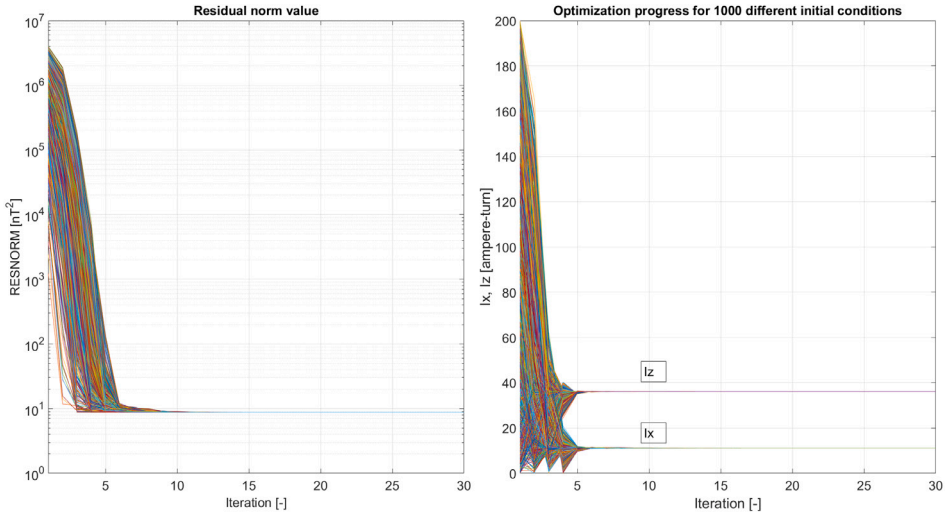

Fig. 19. Optimization convergence.

Appendix A. Supplementary data

Supplementary material related to this article can be found online at https://doi.org/10.1016/j.jmmm.2023.170898.

References

[1] J.J. Holmes, Exploitation of a Ship's Magnetic Field Signatures, San Rafael, Calif, 2006.

[2] J.J. Holmes, Reduction of a Ship's Magnetic Field Signatures, San Rafael, Calif, 2008.

[3] J.J. Holmes, Modeling a ship's ferromagnetic signatures, Synth. Lect. Comput. Electromagn. 2 (1) (2007) 1–75, http://dx.doi.org/10.2200/S00092ED1V01Y200706CEM016, URL https://www.morganclaypool.com/doi/abs/10.2200/S00092ED1V01Y200706CEM016.

[4] A. Kildishev, J. Nyenhuis, Multipole imaging of an elongated magnetic source, IEEE Trans. Magn. 36 (5) (2000) 3108–3111, http://dx.doi.org/10.1109/20.908701.

[5] S.A. Synnes, P.A. Brodtkorb, Representing the ship magnetic field using prolate spheroidal harmonics –A comparative study of methods, pp. 8.

[6] K. Jakubiuk, P. Zimny, M. Wołoszyn, Multidipoles model of ship's magnetic field, Int. J. Appl. Electromagn. Mech. 39 (1–4) (2012) 183–188, http://dx.doi.org/10.3233/JAE-2012-1459, URL https://content.iospress.com/articles/international-journal-of-applied-electromagnetics-and-mechanics/jae01459.

[7] J. Tarnawski, T. Rutkowski, M. Woloszyn, A. Cichocki, K. Buszman, Magnetic signature description of ellipsoid-shape vessel using 3D multi-dipole model fitted on cardinal directions, IEEE Access 10 (2022) 1, http://dx.doi.org/10.1109/ACCESS.2022.3147138.

[8] J. Tarnawski, A. Cichocki, T.A. Rutkowski, K. Buszman, M. Woloszyn, Improving the quality of magnetic signature reproduction by increasing flexibility of multi-dipole model structure and enriching measurement information, IEEE Access 8 (2020) 190448–190462, http://dx.doi.org/10.1109/ACCESS.2020.3031740.

[9] A. Sheinker, B. Ginzburg, N. Salomonski, A. Yaniv, E. Persky, Estimation of ship's magnetic signature using multi-dipole modeling method, IEEE Trans. Magn. 57 (5) (2021) 1–8, http://dx.doi.org/10.1109/TMAG.2021.3062998.

[10] J. Tarnawski, K. Buszman, M. Woloszyn, T.A. Rutkowski, A. Cichocki, R. Józwiak, Measurement campaign and mathematical model construction for the ship zodiak magnetic signature reproduction, Measurement 186 (2021) 110059, http://dx.doi.org/10.1016/j.measurement.2021.110059, URL https://www.sciencedirect.com/science/article/pii/S0263224121009842.

[11] J.-O. Hall, H. Claésson, J. Kjäll, G. Ljungdahl, Decomposition of ferromagnetic signature into induced and permanent components, IEEE Trans. Magn. 56 (2) (2020) 1–6, http://dx.doi.org/10.1109/TMAG.2019.2953860.

[12] O. Somsen, G. Wagemakers, Separating permanent and induced magnetic signature: A simple approach, 2015, Undefined, URL https://www.semanticscholar.org/paper/Separating-Permanent-and-Induced-Magnetic-A-Simple-Somsen-Wagemakers/8d8e0052ffc096a489a544290b9d6246865261ef.

[13] S.H. Im, H.Y. Lee, H.J. Chung, G.S. Park, A study on the effective deperming protocol considering hysteresis characteristics in ferromagnetic material, J. Magnetics 23 (4) (2018) 680–688, http://dx.doi.org/10.4283/JMAG.2018.23.4.680, URL http://www.dbpia.co.kr/Journal/ArticleDetail/NODE07585142.

[14] H.S. Ju, H.J. Chung, S.H. Im, D.W. Jeong, J.W. Kim, H.B. Lee, G.S. Park, Efficient deperming protocols based on the magnetic properties in demagnetization process, IEEE Trans. Magn. 51 (11) (2015) 1–4, http://dx.doi.org/10.1109/TMAG.2015.2436703.

[15] S.-H. Im, H.-Y. Lee, G.-S. Park, Novel deperming protocols to reduce demagnetizing time and improve the performance for the magnetic silence of warships, Energies 14 (19) (2021) 6295, http://dx.doi.org/10.3390/en14196295, URL https://www.mdpi.com/1996-1073/14/19/6295.

[16] T. Baynes, G. Russell, A. Bailey, Comparison of stepwise demagnetization techniques, IEEE Trans. Magn. 38 (4) (2002) 1753–1758, http://dx.doi.org/10.1109/TMAG.2002.1017767.

[17] J.-W. Kim, S.-H. Kim, J.-h. Kim, H.-B. Lee, H.-J. Chung, Efficient search method of deperming protocol for magnetic silence of vessel, J. Magnetics 22 (1) (2017) 85–92, http://dx.doi.org/10.4283/JMAG.2017.22.1.085, URL http://koreascience.or.kr/article/JAKO201713842135008.page.

[18] S.H. Im, Efficient flash-D deperming protocol for magnetic stealth of submarine using the preisach model, Energies 15 (7) (2022) 2587, http://dx.doi.org/10.3390/en15072587, URL https://www.mdpi.com/1996-1073/15/7/2587.

[19] M. Birsan, Simulation of a ship's deperming process using the Jiles–Atherton model, IEEE Trans. Magn. (2021) http://dx.doi.org/10.1109/TMAG.2021.3068555.

[20] M. Wołoszyn, P. Jankowski, Ship's de-perming process using coils lying on seabed, Metrol. Measur. Syst. 26 (3) (2019) http://dx.doi.org/10.24425/mms.2019.129582, URL http://yadda.icm.edu.pl/baztech/element/bwmeta1.element.baztech-72fedfa5-1aa8-4f61-b766-325a0d576547.

[21] V. Modagekar, S.A. Karim, N. Singh, F. Kazi, Optimization in tri-axial degaussing system design and estimation of degaussing coil currents, IEEE Trans. Magn. 53 (4) (2017) 1–12, http://dx.doi.org/10.1109/TMAG.2016.2642890.

[22] D. Tian, S.-d. Liu, Z.-x. Li, A ship's magnetic field camouflage method based on multi-objective genetic algorithm, Vibroeng. Procedia 11 (2017) 135–139, http://dx.doi.org/10.21595/vp.2016.17971, URL https://www.extrica.com/article/17971.

[23] N.-S. Choi, G. Jeung, C.-S. Yang, H.-J. Chung, D.-H. Kim, Optimization of degaussing coil currents for magnetic silencing of a ship taking the ferromagnetic hull effect into account, IEEE Trans. Appl. Superconduct. - IEEE Trans. Appl. Superconduct. 22 (2012) 4904504, http://dx.doi.org/10.1109/TASC.2011.2180296.

[24] N.-S. Choi, G. Jeung, S.S. Jung, C.-S. Yang, H.-J. Chung, D.-H. Kim, Efficient methodology for optimizing degaussing coil currents in ships utilizing magnetomotive force sensitivity information, IEEE Trans. Magn. 48 (2) (2012) 419–422, http://dx.doi.org/10.1109/TMAG.2011.2177515.

[25] D.-W. Kim, S.-K. Lee, B. Kang, J. Cho, W. Lee, C.-S. Yang, H.-J. Chung, D.-H. Kim, Efficient re-degaussing technique for a naval ship undergoing a breakdown

in degaussing coils, J. Magnetics 21 (2) (2016) 197–203, http://dx.doi.org/10.4283/JMAG.2016.21.2.197, URL http://koreascience.or.kr/journal/view.jsp?kj=E1MGAB&py=2016&vnc=v21n2&sp=197.

[26] P. Leliak, Identification and evaluation of magnetic-field sources of magnetic airborne detector equipped aircraft, IRE Trans. Aerosp. Navig. Electron. ANE-8 (3) (1961) 95–105, http://dx.doi.org/10.1109/TANE3.1961.4201799, Conference Name: IRE Transactions on Aerospace and Navigational Electronics.

[27] Reveal the world we live in | SIMULIA – Dassault Systèmes, URL https://www.3ds.com/products-services/simulia/.

[28] Least-squares (model fitting) algorithms - MATLAB & simulink, URL https://www.mathworks.com/help/optim/ug/least-squares-model-fitting-algorithms.html.

[29] scipy.optimize.least_squares — SciPy v1.9.3 Manual, URL https://docs.scipy.org/doc/scipy/reference/generated/scipy.optimize.least_squares.html.

[30] Ceres solver — A large scale non-linear optimization library, URL http://ceres-solver.org/.

[31] Excel solver - limitations on smooth nonlinear optimization, 2011, Solver, URL https://www.solver.com/excel-solver-limitations-smooth-nonlinear-optimization.